CrossMark

ORIGINAL ARTICLE

Coupling of shear–circumferential stress pulses investigation through stress phase angle in FSI models of stenotic artery using experimental data

Milad Samaee[1] · Mohammad Tafazzoli-Shadpour[2] · Hamed Alavi[3]

Abstract Many cardiovascular diseases are closely associated with hemodynamic parameters. The main purpose of this study is mimicking a physiological blood flow in stenotic arteries to provide an understanding of hemodynamic parameters. An experimental setup was designed to produce original pulsatile flow and measure pressure pulse waves through a compliant tube. Moreover, a numerical model considering fluid–solid interaction was developed to investigate wall shear stress and circumferential stress waves, based on the results of the experiments. Results described elevated mean pressure by increasing stenosis severity especially at the critical obstacle of 50 %, which the pressure rose significantly and raised up by 10 mm Hg that may cause damage in endothelial cells. Increasing in stenosis severity led to: more negative wall shear stress and more oscillation of shear stress at the post-stenotic region and also more absolute value of angular phase difference between wall shear stress and circumferential stress waves at the stenotic throat. All of the aforementioned parameters determinant the endothelial cell pathology in predication of potential sites of progression of atherosclerotic plaques. Therefore, results can be applied in study of plaque growth and mechanisms of arterial remodeling in atherosclerosis.

1 Introduction

Atherosclerosis is a major vascular disease and remains the leading cause of world mortality [9, 14]. It has been widely accepted that cardiovascular diseases are associated with hemodynamic conditions [20]. Hemodynamic parameters contribute to the initiation, localization and development of stenosis as a major health risk [1, 17, 38]. Some of the mechanical parameters that have been verified to be associated with development of arterial stenosis are as follows: hypertensive pulsatile blood pressure and high cyclic circumferential stress (CS) on arterial wall [6], disturbed flow patterns [15], low, excessive and highly oscillating wall shear stress (WSS) [2, 4, 37], temporal variation of the shear stress [26] and spatial wall shear stress gradient [18].

Among the abovementioned parameters, mean wall shear stress (time-averaged WSS) and oscillatory shear index (OSI) are two critical parameters, which play important roles in mechanics of atherosclerosis [28, 30, 34]. From the pathological point of view, in some regions such as bifurcations and stenotic sites, OSI has been shown to be relatively high and mean WSS relatively low compared to nearby sites [34]. In addition to the direct influence of wall mechanics and fluid dynamics, mechanical stresses are influenced by wall–flow interactions. Because of the flexibility of arteries, the arterial wall displacement, which is caused by the pressure pulse, affects the blood flow pattern. Theoretical considerations of interactions between elastic wall and blood flow significantly affect characteristics of flow field and wall domain and therefore influence hemodynamic parameters, particularly pulsatile wall shear stress,

✉ Mohammad Tafazzoli-Shadpour
   tafazoli@aut.ac.ir

1   Mechanical and Aerospace Engineering Department,
    Oklahoma State University, Stillwater, OK, USA

2   Cardiovascular Engineering Lab., Faculty of Biomedical
    Engineering, Amirkabir University of Technology, Tehran,
    Iran

3   Department of Biomedical Engineering, University
    of California, Irvine, CA, USA

Fig. 1 Schematic representation of the experimental setup, which is included a closed loop and Windkessel model (elastic and resistant elements, pulsatile pump and reservoir)
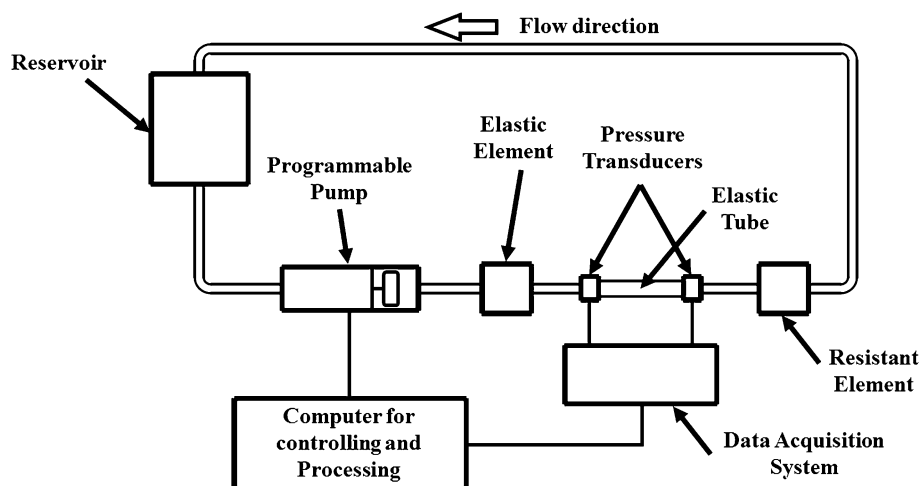
and pressure gradient waves in both healthy and stenotic arteries [27].

A considerable number of studies, both experimental and computational, have investigated effects of hemodynamic parameters on blood flow and development of arterial diseases [15, 27–29, 33, 36, 41]. Although scholars have attempted to conduct experiments on cardiovascular diseases, they performed under simplifying assumptions overlooking some parameters such as physiological flow condition, wall elasticity and fluid–wall interaction. Such experiments focused on the flow downstream of the stenosis, and particularly on the disturbances induced by the stenosis; however, they failed to consider the effects of wall elasticity [23]. However, most studies focused on the conditions which may be related to artery collapse and plaque cap rupture such as considerable compressive stress in the tube wall and critical flow conditions like negative pressure, high shear stress and flow separation [36].

Fluid–structure interaction (FSI) modeling and computational methods have been extensively employed in the study of cardiovascular function and pathology, and also blood flow characteristics through stenotic arteries have been investigated under different assumptions [15, 27–29, 36]. In most studies blood flow has been restricted by some assumptions such as steady flow [3, 36]; models of stenotic arteries as rigid-walled tubes [3, 11] compliant wall under static no-flow conditions [13, 22]; or disregarding effects of arterial wall–blood interactions [3, 20]. The scope of the aforesaid investigations was not extended into two parameters: (1) the relation between stenosis severity and shear stress pulse and (2) the angular phase difference between wall shear stress and circumferential stress waves due to elastic wall–fluid coupling. These two parameters seem to be determinants of endothelial cell pathology in predication of potential site of stenotic plaque growth [8].

The main purpose of this study is to provide a more accurate understanding of hemodynamic parameters of blood flow in models of stenotic arteries, considering nearly realistic conditions of physiological blood flow. An experimental setup was designed and developed to produce original pulsatile arterial flow. This setup is capable of monitoring and measuring blood pressure waves for carrying out experiments in different scales of symmetric stenosis using a compliant tube similar to an elastic artery. Moreover, a numerical model considering effects of FSI was developed to investigate wall shear stress, circumferential stress waves and the phase shift between them, based on the output of experimental setup. Given the concept of stress phase angle, the wall–blood coupling was studied through interaction of pressure flow pulses, and the consequent cyclic shear and circumferential stress values were evaluated. The results can provide a useful means to extend scope of effects of stenosis on hemodynamic parameters and mechanisms involved in plaque growth.

2 Methods

2.1 Experimental setup

The setup is shown in Fig. 1, and it is capable of producing a flow wave similar to that of an original physiological blood flow in desired arteries and also detecting and measuring the consecutive blood pressure and pressure difference waves in real time (Fig. 1), given the flow wave pattern as the input. For the current study, a model of the brachial artery was chosen due to the availability of its physiological flow wave and pressure pulse data, together with its mechanical and geometrical parameters. In addition, the brachial artery is highly compliant and the effects

of elasticity of the wall on flow patterns are prominent. Within the human body most of the arteries are less distensible; however, even in those cases it is important to know how the compliance of that artery might contribute to the flow regime specifically when luminal obstruction is involved. Hence, although brachial arteries are less prone to atherosclerotic plaque formation, for a typical distensible artery the influence of wall elasticity on the flow can be studied when the artery is obstructed with different scales of stenosis. See Appendix for more details about the experimental setup.

2.2 Experimental protocol

Before running each experiment, the pump was discharged of any remaining bubbles using discharge valves arrayed on both transducers. Calibration of the pump was then accompanied to minimize probable errors in producing the original flow and in measurement system using *Chart for Windows™ v5.0.1* software, which the output signals of the transducers were adjusted to the real numerical values.

The initial experiment simulated the flow in a healthy brachial artery. The blood flow wave of brachial artery was set to the pump to produce an original arterial pulsatile flow [24]. Mean flow rate, $\dot{Q}$, was equal to 3.66 (ml s^{-1}), and the frequency of the wave, ω, was 1.16 (Hz) (70 heart BPM). The fluid (a mixture of water, 65 % by weight; glycerin, 35 % by weight) was chosen to be a Newtonian fluid with a viscosity of $\mu = 3.5$ (cP) and density of $\rho = 1050$ (kg m^{-3}), to mimic the density and viscous properties of blood in large arteries [12]. The dimensionless parameters of Reynolds (Re) and Womersley (N_w) numbers for flow in this experiment were calculated as 297 and 1.4, respectively. The values comply with published data for physiological flow conditions of the same level arteries and are in close analogy.[35] The inlet, P_1, and outlet, P_2, pressure waves were detected by means of the data acquisition and processing system, and consequently the pressure difference wave was calculated.

The main experiment was designed and performed with the aim to study the effect of different scales of symmetric stenosis on pressure and pressure difference waves with assumption of constant flow to distal part. The characteristics of the flow wave and the setup were maintained consistent with the previous experiment, except different scales of symmetric stenosis were set to the elastic tube. The stenosis profiles were generated by external constraints around the wall of elastic tube as described above and shown in Fig. 2. The degree of stenosis severity was defined as the degree of reduction in cross-sectional area of lumen, varied as 5, 10, 20, 30, 50, 60, 70 and 80 % to investigate effects of stenosis severity on hemodynamic parameters. To avoid the circumferential effects on deformation within the stenotic

site and altered velocity pattern, boundary conditions were allocated far enough.

2.3 Numerical analysis

The governing equations in fluid domain (continuity and momentum conservation) for non-Newtonian modified Casson model, in solid wall (elastodynamics equations), and also fluid–solid coupling are considered in this study, which are all discussed in detail in the appendix. Also the numerical modeling and boundary conditions are discussed in the appendix.

To verify accuracy of numerical simulation, results for effective stresses at stenotic throat in different stenosis severities (20, 50 and 70 %) were compared to the published numerical results of Valencia and Baeza's (2009) [39] using ADINA software. All computational models including elastic modulus, lengths, density, profile of stenosis and viscosity of fluid were considered similar to those used in Valencia and Baeza's. The given results from our simulation describe good agreements as shown in Fig. 3a. Moreover, minimum and maximum effective stresses at pre-stenotic zone for the stenosis severity of 50 % were calculated to be 52.3 (kPa) and 88.1 (kPa), respectively, comparable to the reported values of 55 (kPa) and 84.9 (kPa) [39]. Additionally, acceptable compatibility was achieved between results of WSS in this study compared to those of Kaazempur-Mofrad et al. [16] (Fig. 3b).

3 Results

3.1 Experimental results for models of stenosed arteries with different severities

In accordance with experimental conditions, the results for inlet and outlet pressure waves (P_1 and P_2) for normal and stenosed models with degrees of severities from 5 to 80 % are presented in Fig. 4a, b. Although luminal obstruction causes change in the inlet and outlet pressure waves, the elevation of P_1 is dominant and changes in P_2 are less noticeable.

In addition to the inlet and outlet pressure waves, luminal obstruction influences the pressure difference wave. The pressure difference wave was evaluated by subtracting the outlet (P_2) and inlet (P_1) pressure waves in real time, measured by pressure transducers simultaneously. The resultant pressure difference waves are shown in Fig. 4c. The pressure drop is more intensified when the severity is elevated. Such effect is highly prominent in higher grades of stenosis. The increased pressure difference is due to increase in the resistance against the flow by stenosis. Additionally, increased severity results in rightward shift of
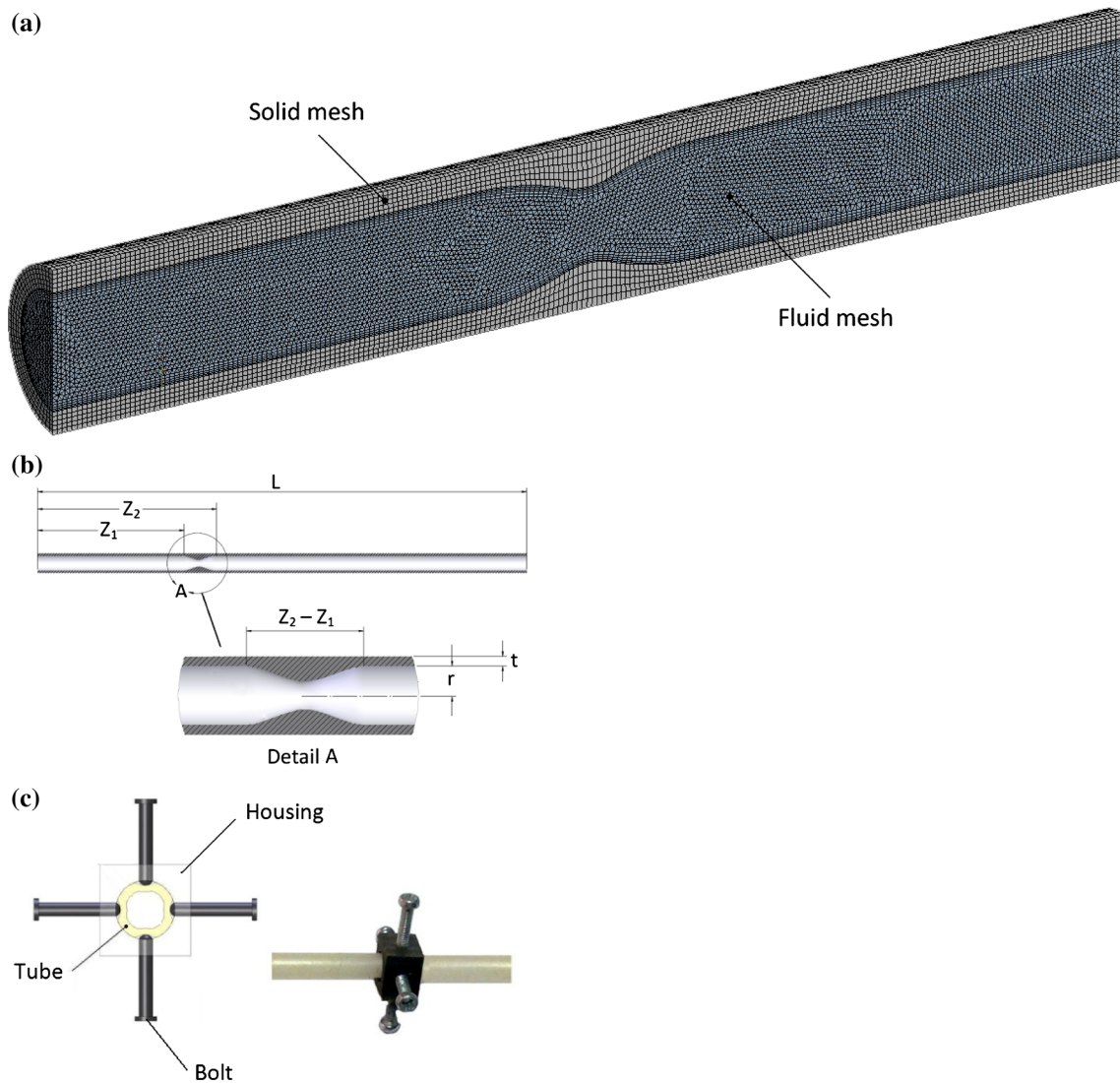
Fig. 2 **a** Transverse section of the meshed model, which was used in numerical modeling, the wall section has 8-node hexahedral mesh and the fluid field has 4-node tetrahedral mesh (see appendix). **b** Geometry of the total model, including the stenotic area. Z_1 and Z_2 are longitudinal distances of start and end of stenosis from the tip of arterial model, respectively, and the length of stenosis is shown in Detail A. r and t are internal radius and thickness of the tube, respectively. **c** External housing and bolts for creation of the stenosis

peak of pressure difference as demonstrated in Fig. 4c. The resultant pressure waves have been obtained from different operating cycles of the pump and hence are presented in averaged values. Due to accumulation of results figures are not provided with error bars. To demonstrate deviation of results, Fig. 4d shows pressure waves for a typical model with stenosis severity of 60 % with error bars. The rest of results indicate deviations within almost the same range.

The mean values of inlet pressures are calculated and presented in Fig. 4 for different degrees of stenosis. In lower scales of stenosis (lower than 60 %), alterations in the magnitude of mean inlet pressure are small, beyond that changes are considerable. Hence, to maintain a certain flow due to metabolic requirements of distal tissues, the

pressure difference and inlet pressure have to be elevated. The significant rise in the inlet pressure is highly prominent after specific degree of stenosis, in current study about 60 % (Fig. 5). Such degree of stenosis describes a critical condition, beyond which the mean inlet pressure has to be elevated significantly to maintain the flow.

3.2 Numerical results for FSI models of stenosed arteries with different severities

3.2.1 Model verification

Resultant P_1 values obtained from numerical modeling with boundary conditions of P_2 and flow waves as experimental
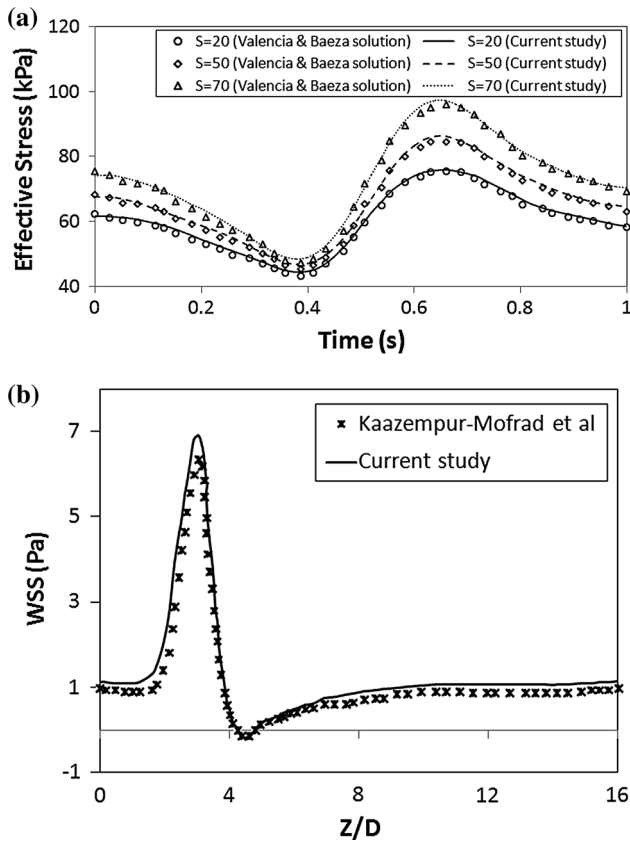
Fig. 3 Numerical validation: **a** comparison of time variation of effective stress for three different stenosis severities at stenotic throat with Valencia et al. study, **b** comparison of WSS along the axisymmetric stenotic artery (z) with $S = 56$ % and Reynolds number = 250 with Kaazempour-Mofrad et al. study

parameters are presented in Fig. 6 for stenosis severities of 20, 50 and 80 %. The P_1 waves resulted from FSI modeling are compared to those obtained from experiments.

Results indicate average values of deviation of 1.1, 1.1 and 1.07 % for models with 20, 50 and 80 % severities, respectively. For maximum values of deviation these values correspond to 4.7, 4.8 and 4 %, respectively. The results of numerical modeling for P_1 values are in reasonable agreement with experimental results, as the waves only differ by the criteria of normalized root mean square deviation of NRMSD = 0.01. The NRMSD is calculated by Eq. 1:

$$NRMSE = \frac{\sqrt{\frac{\sum_{i=1}^{n}(P_{exp,i}-P_{num,i})^2}{n}}}{P_{max} - P_{min}} \tag{1}$$

where n indicates total time steps in each cycle and P_{exp} and P_{num} correspond to experimental resulted and numerical calculated inlet pressures, respectively. Such accordance enables calculation of shear and circumferential stress values based on experimental conditions. To study details

of such stress waves, results are presented and discussed in three separate regions: pre-stenotic, stenotic and post-stenotic. Pre- and post-stenotic regions are defined as 1.5D (1.5 times of lumen diameter) before and after the stenotic region, respectively.

3.3 Wall circumferential stress

Figure 7 illustrates the circumferential stress waves for models with three degrees of stenosis at three sites.

3.3.1 Wall shear stress (WSS)

In contrast to circumferential stress, wall shear stress (WSS) increases significantly at the stenotic throat (Fig. 8).

The conduct of the WSS along the axis of the artery is demonstrated in Fig. 9 through mean shear stress (the average value of shear stress during arterial pulse) and oscillatory shear index (OSI) parameters.

3.4 Angular phase shift

It has been shown that angular phase difference between wall shear stress and circumferential stress waves (stress phase angle, SPA), which an endothelial cell in arterial wall experiences, is a key parameter in endothelial cell pathology [28, 29]. The higher absolute values of SPA describe more critical conditions [28, 29].

Figure 10 indicates magnitudes of SPA based on the experimental results and FSI modeling. The calculation of angular phase difference is based on discrete Fourier transform for the first eight harmonic frequencies, at the stenotic throat for severities of 20, 50 and 80 %.

4 Discussion

Endothelial injury is the major determinant of atherosclerotic plaque formation and progression [8, 42]. Local and systemic hemodynamic factors such as WSS, CS and the phase difference between them contribute to such phenomenon. In this study, the calculated stress values through experimental setup and computational models were in accordance with published data. The range of WSS for specific arteries with 50–56 % stenosis severity has been shown to be −0.2 to 6.5 (Pa) reported by Kaazempour-Mofrad et al. [16] and −0.6 to 5.7 (Pa) reported by Lee and Xu [19]. In this study, such values were within the range of −0.5 to 7 (Pa). The peak WSS value for the healthy common carotid and brachial artery has been proposed to be 3.4 ± 0.8 (Pa) and 3.9 ± 0.8 (Pa) and for the mean WSS value to be 1.15 ± 0.21 (Pa) and 0.48 ± 0.15 (Pa), respectively [7].

Fig. 4 **a** Inlet (P_1), which is elevated by increasing stenosis severity, **b** outlet (P_2) pressure waves, which remained almost unchanged by increasing stenosis severity, **c** pressure difference waves obtained in experiments in different scales of stenosis and **d** inlet, outlet and pressure difference waves with error bars for a typical model ($S = 60$ %)
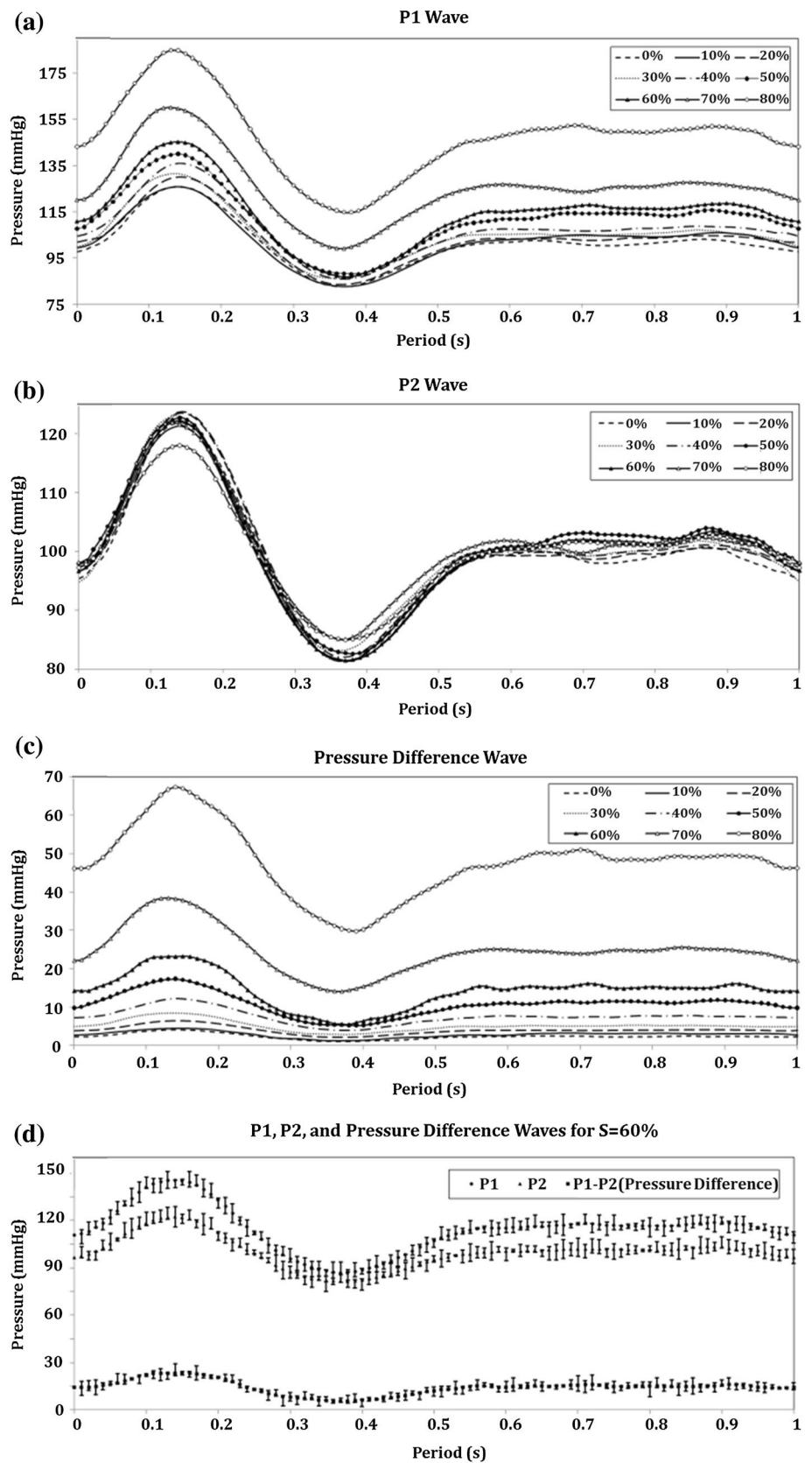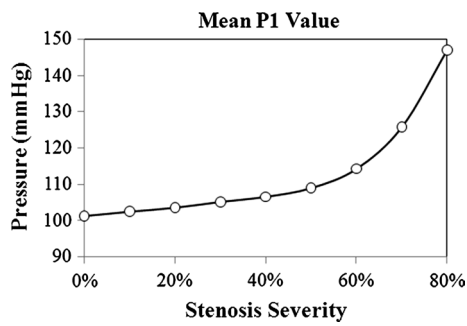
Fig. 5 Effect of elevation of stenosis severity on mean P_1 value. At 50 % stenosis the mean upstream blood pressure increased by 10 mm Hg, which it can be considered as a critical percentage of stenosis severity

Considering flow in cylindrical tubes, pressure gradient is mostly sensitive to the tube radius. Local decrease in luminal radius due to elevation of severity leads to the increase of pressure gradient. In current study, flow regime was set to resemble physiological conditions where the pressure in arterial tree is regulated to maintain blood flow through stenotic arteries for metabolic requirements. If the flow rate has to be constant due to downstream metabolic requirements, the pre-stenotic pressure and pressure difference rise (Fig. 4b, c). To keep flow constant, as described by numerical modeling, the inlet pressure has to be elevated. The increase in the upstream pressure, to compensate resistance of stenosis, leads to elevation of pressure of parallel non-stenotic arteries. If the rise of pressure is

Fig. 6 Comparison of experimental and numerical inlet pressure waves for 20, 50 and 80 % stenosis severity. All the comparisons show a good agreement between numerical and experimental approaches
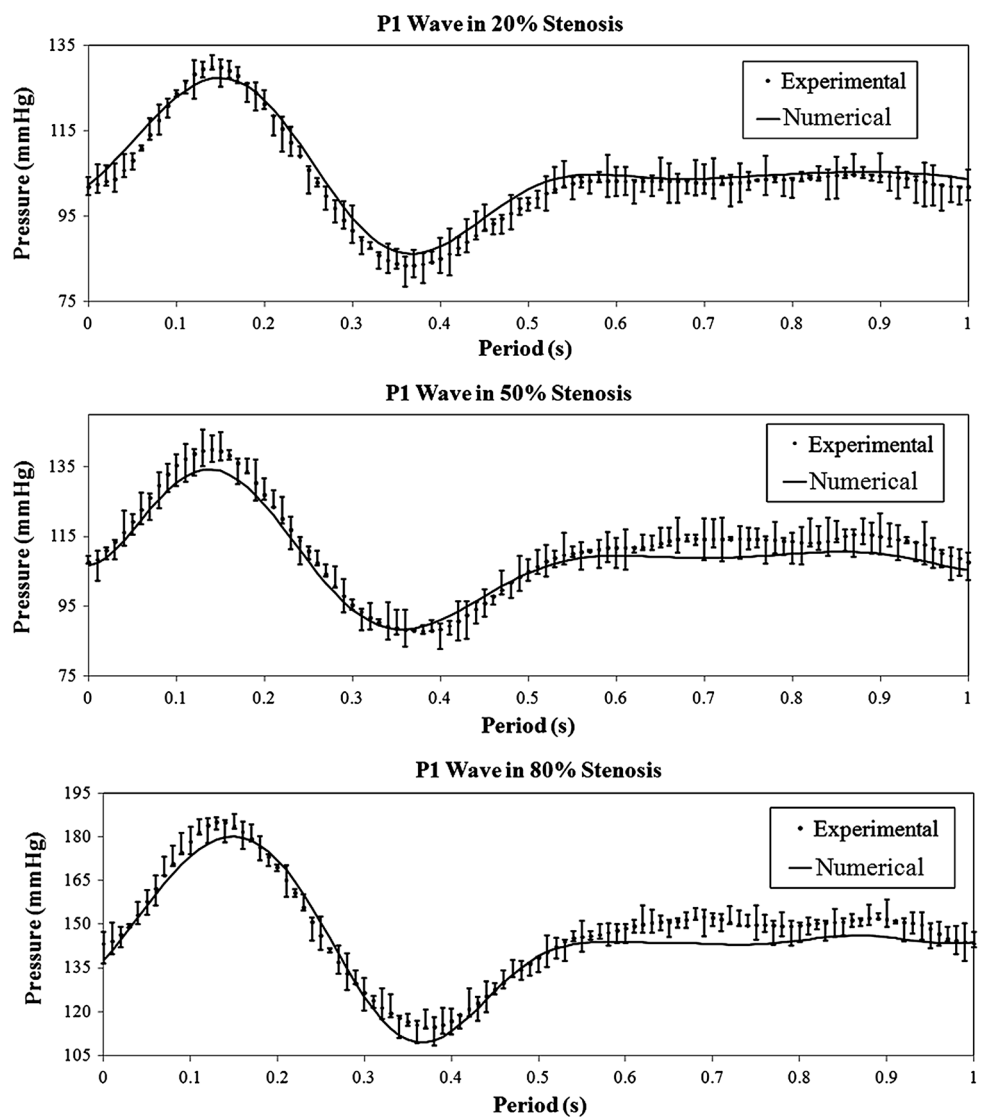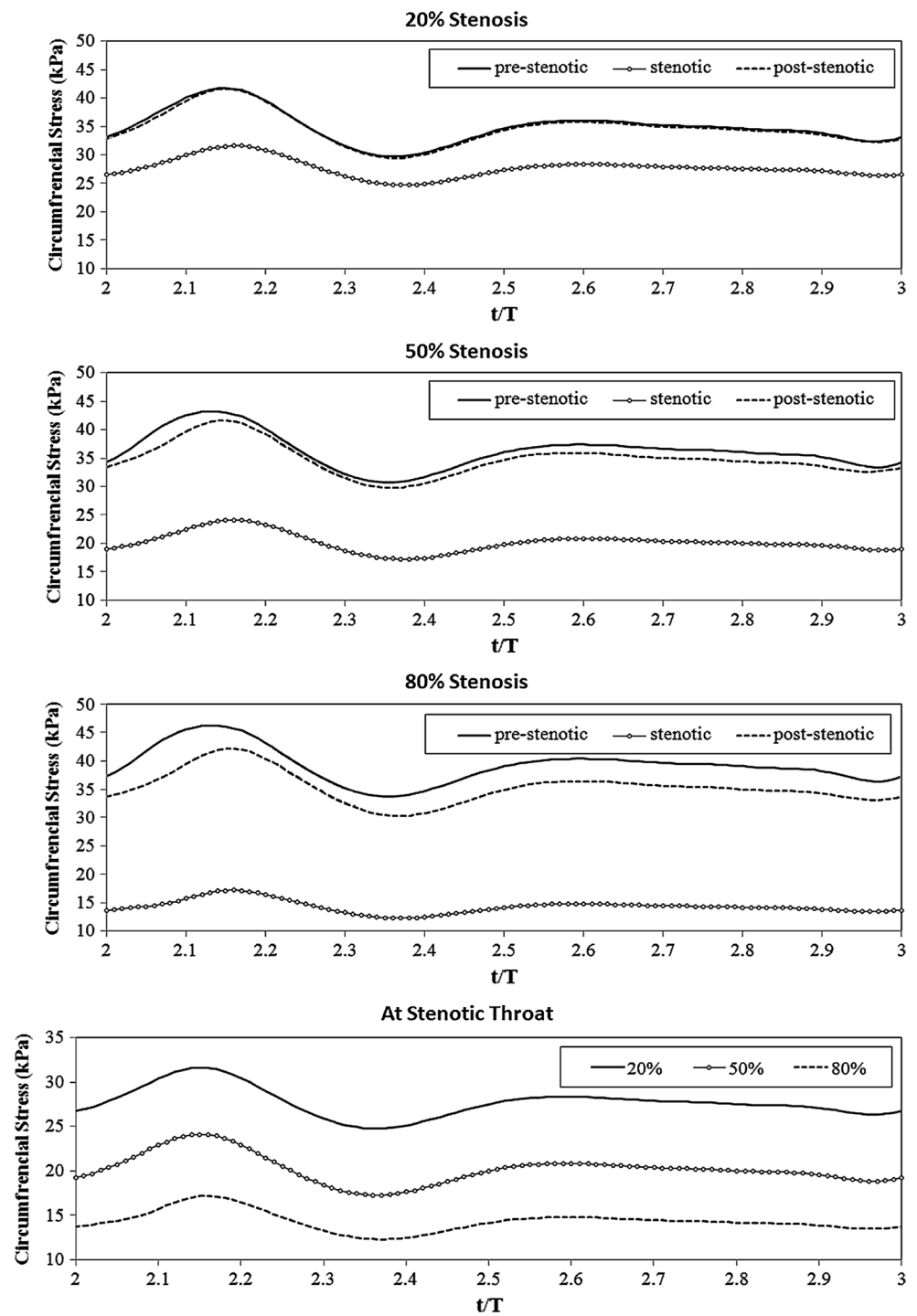
significant due to the critical severity, a systemic hypertension is manifest in real biological conditions. By assumption of constant flow rate, if the inlet pressure is elevated excessively, it is assumed that such trend cannot be maintained due to effects on systemic pressure. Hence, to avoid such pressure rise, flow rate may decrease. This means that by increase of stenosis severity, until the inlet pressure reaches the critical point, the flow is set almost constant.

However, further increase in severity leads to blood deficiency to avoid systemic hypertension.

The degree of critical severity might vary among different arterial sites. Such degree depends on local geometry and hemodynamic parameters. In this study, the critical severity occurred almost at 50 %, which cased to 10 mm Hg elevation in upstream blood pressure. Based on previous studies, 10 mm Hg pressure increase may result in

Fig. 8 Comparison of wall shear stress pulses for stenosis severities of 20, 50 and 80 % (all diagrams are normalized to the peak WSS). By increasing stenosis severity, the WSS at stenotic throat increased significantly and became more negative at post-stenotic region
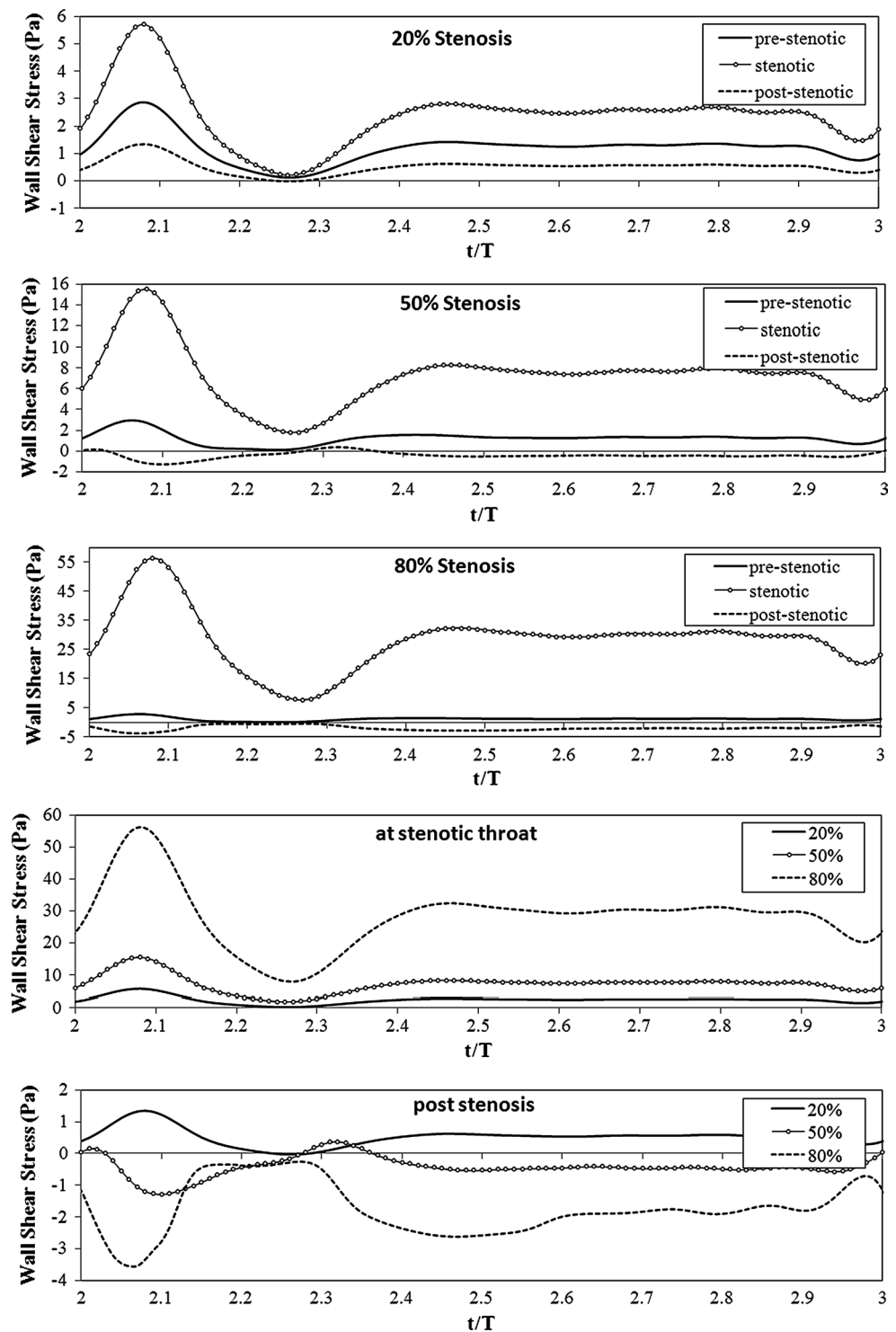
endothelial cells damage [10]. For severities smaller than 50 %, to maintain flow rate, the inlet pressure increase was less than 3 %. However, a further elevation of severity from 50 to 70 % caused an extra increase of 14 % in inlet pressure. The value of critical severity changes when the radius of artery and the value of blood flow are altered. In other words, the critical degree of severity depends on arterial

site. Study of such value is of great importance in major arteries at risk, such as coronary and carotid arteries.

While in general, by elevation of stenosis severity, the maximum and minimum values of circumferential stress waves (31.5–43 (kPa)) remained constant in pre-stenotic site, such values were reduced in stenotic regions (from the range of 31.5–43 (kPa) non-stenotic model to 13–17.5

Fig. 9 Mean wall shear stress and oscillatory shear index along the artery axis in the model with different stenosis severities. There is a peak value of mean WSS at stenotic region, and it became more severe by increasing stenosis. Also, the OSI became wider in 80 % stenosis compared to lower stenosis
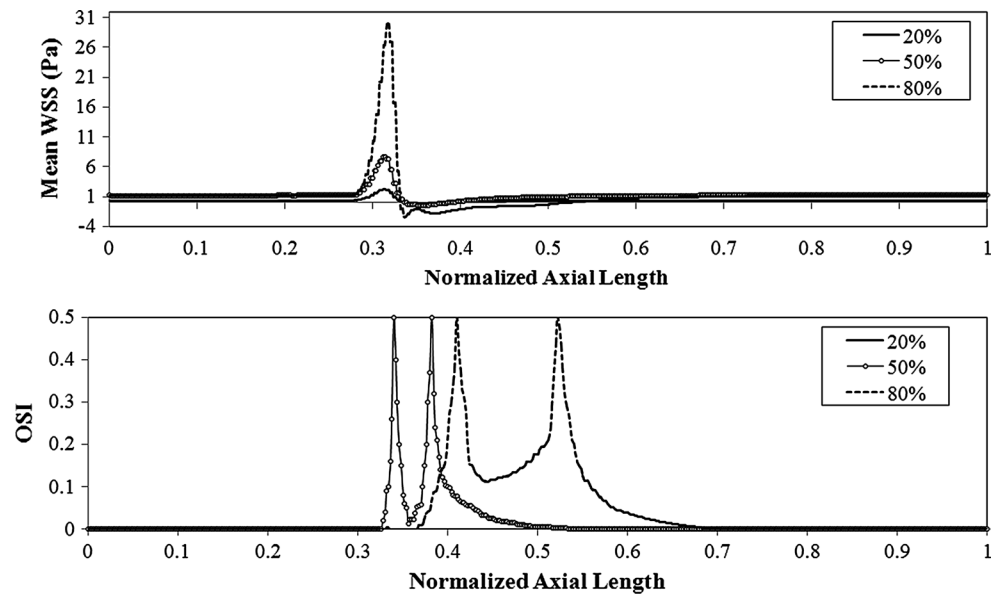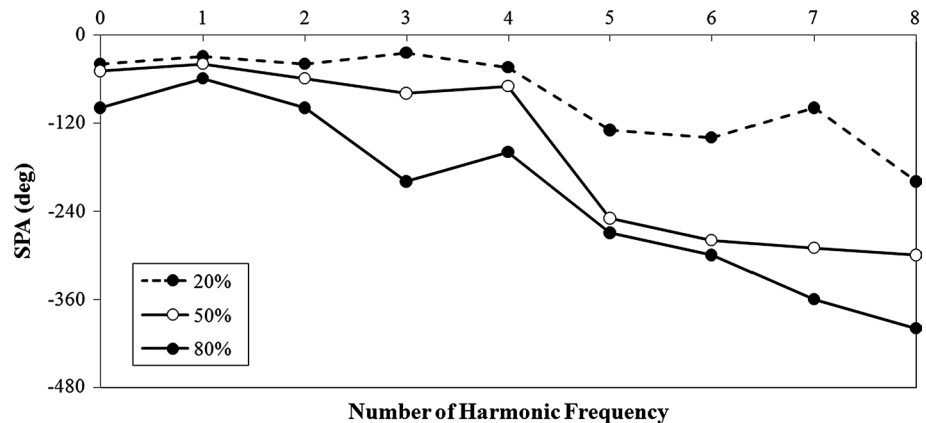

Fig. 10 Angular phase difference between wall shear stress and circumferential stress waves, for first eight harmonic frequencies at post-stenotic region. SPA values became more negative in more severe stenosis

(kPa) for 80 % stenosis severity) due to increased plaque thickness which makes the wall displacement smaller (from 1.1×10^{-6} (m) to 3.9×10^{-7} (m) at the peak value) and consequently the stress level smaller.

The circumferential stress pulse amplitude at the stenotic site decreased significantly as the stenosis was elevated by the amounts of 8.3, 6.6 and 4.7 (kPa) for $S = 20$, 50 and 80 %, respectively, but it almost remained constant (11.5 (kPa)) at pre-stenotic region. Hence, for higher values of luminal obstruction, the variation of circumferential stress along the lumen axis is more prominent.

In post-stenotic section, small reductions in circumferential stress are observed. This is due to sharp pressure drop in more severe stenotic region, which leads to lower maximum post-stenotic pressure and consequently lower circumferential stress. In critical conditions with significant pressure drop the post-stenotic neighborhood undergoes collapse [43]. In current study, for the model with 80 %

severity, the minimum value of post-stenotic CS was as low as 30 kPa, while the values of CS at pre-stenotic region remained almost constant. For idealistic models with high values of pressure gradient, significant collapse has been shown to occur in post-stenotic region [36].

In contrast to circumferential stress, wall shear stress (WSS) increased significantly at the stenotic throat (Fig. 8). Such increase was markedly intensified by elevated severity. Both maximum shear stress value and shear stress pulse amplitude were elevated by increased severity. The magnitude of maximum shear stress increased 171 % from 20 to 50 % severity and 262 % from 50 to 80 % severity, and shear stress pulse amplitude increased 150 % from 20 to 50 % and 253 % from 50 to 80 % severity. Additionally, by elevation of stenosis severity, a more negative WSS was observed at post-stenotic site. As can be inferred by negative values of WSS in Fig. 8, increased severity induced more back flow and vortexes in post-stenotic region. For

the severity of 80 %, the peak value of WSS dropped to −3.7 Pa which might contribute to endothelial injury and plaque progression in axial direction. For higher values of luminal obstruction WSS fluctuated mostly with negative values, describing potential pathological outcome such as endothelial injury and post-stenotic axial plaque growth [34].

The post-stenotic high variation of mechanical stresses induced by stenosis severity manipulates the phase difference between shear and circumferential stresses. Since WSS was reduced and the circumferential stress was elevated at the post-stenotic site, as the stenosis of artery became more severe, the stress gradient was intensified along the axis of tube with higher severities resulting in altered phase difference and possible pathological consequences. Models with high grade of stenosis showed higher elevation of WSS value at stenosis and higher reduction of WSS distal to plaque.

Alteration in WSS pattern caused by disturbed blood flow is a major determinant of endothelial damage along the arterial tree through altered permeability to LDL and other large molecules, platelet activation and aggregation [31]. Changes in WSS modulate diameter adaptive responses, intimal thickening and thrombosis [31]. Maximum WSS occurred at the throat of the stenosis. Very high shear stress values may contribute to endothelial injury and be related to platelet activation and aggregation [4, 31]. Results showed that in higher stages of stenosis severity, WSS values (both maximum value and stress wave amplitude) were significantly elevated. Figure 8 shows WSS wave at stenotic throat for different scales of stenosis. Unlike circumferential stress, shear stress pulse is increased. For a highly obstructed model (severity of 80 %) the value of WSS is within the range of published data for endothelial damage.

Low and in some cases negative shear stress trigger plaque formation and further growth of initiated plaques [21]. In the post-stenotic region, WSS is reduced leading to a negative value for high grades of stenosis (Fig. 8). Models with high grade of stenosis result in sharper reduction of WSS distal to plaque and more intense fluctuation during pressure pulse. Recirculation zones as a result of shear stress patterns downstream of the tube intensify possibility of transferring large molecules within the wall, including lipids, which often are found in plaque composition [21]. Patterns of WSS in post-stenotic region shown in Fig. 8 suggest that the vulnerable site of further plaque formation and progression is the post-stenotic neighborhood. This is in agreement with findings that the post-stenotic segment is of more pathological importance [26] and higher possibility of endothelial injury and plaque growth to even more luminal obstruction before plaque rupture [4, 31].

At the systolic peak for the stenotic arteries, WSS at the inner wall peaks at the neck of the stenosis reaches the minimum value in the post-stenosis section and then gradually recovers downstream until it levels off. The more severe stenosis is the further down the location of minimum WSS along the inner wall of the artery. The WSS at the inner wall is significantly influenced by the presence and severity of the stenosis (Fig. 9), especially in the post-stenosis site. Additionally, the magnitude of OSI in the post-stenosis region is noticeable especially for the higher degrees of severity as it increases by elevation of luminal obstruction. The high magnitude of OSI and low and even negative values of shear stress after luminal obstruction suggest the possible post-stenotic endothelial injury and progression of the stenosis downward. It has been shown that OSI values near 0.5 describe the situation in which WSS exceedingly fluctuates with higher possibility of endothelial damage [35]. In this study, severities of 50 to 80 % describe such situation.

As the stenosis becomes more severe, the angular phase difference at first harmonic frequency tends to become more negative at the post-stenotic site. Such trend at higher scales of stenosis leads to critical environment on endothelium, which suggests potential post-stenotic endothelial injury and axial plaque growth [28]. As SPA values become lower than −180 degree, increased LDL and possible endothelial injuries have been proposed [25, 35]. In this study, as described in Figs. 8, 9 and 10, the negative values of SPA are closely correlated with negative values of WSS.

5 Conclusion

By conducting experiments, we found that increased severity of luminal obstruction led to elevated inlet pressure. In lower scales of stenosis, the pressure rise was minor, but as the cross section of the lumen was reduced to a critical level, the pressure rose significantly. In this study we found that the critical severity was evaluated to be nearly 50 %. The negative values of shear stress, high fluctuations of shear stress, together with more negative angular phase difference in the first harmonic frequency, might be key parameters in predicting potential sites for endothelial injury and subsequently plaque growth. The negative value of WSS will cause flow separation in post-stenotic region and may result in further growth of plaque [32]. The angular phase difference between wall shear stress and circumferential stress waves became more negative at post-stenotic region as the degree of stenosis severity was elevated. The shear stress also became more negative with higher fluctuations in post-stenotic section as the scale of stenosis was raised. The trend of alteration in parameters was intensified for higher degrees of stenosis. Such parameters seem to be determinants of endothelial cell pathology and thrombus formation and predication of potential progression sites

of the plaque. In this study, post-stenotic neighborhood was shown to be the location in which all three major determinants (negative WSS, high OSI and negative SPA) reach their critical values. This is in agreement with physiological findings, as it has been reported that the plaques tend to grow in directions distal to stenotic region [26, 37]. The results can be applied in the study of plaque maturity and growth, leading to clinical consequences of atherosclerosis.

Glossary

OSI   Oscillatory shear index. It is a parameter that shows us how much the wall shear stress changed in direction and magnitude (non-dimensional)

SPA   Stress phase angle. The phase angle difference between the first harmonic of pressure and wall shear stress (degree)

Appendix: More details on the experimental setup

An overall view and schematic representation of the experimental setup for simulation of blood flow in elastic arteries is shown in Fig. 11. The setup consists of three major components: programmable pulsatile flow pump, elastic tube and the data acquisition and processing system.

A custom-made pump was designed and manufactured to generate pulsatile flow in a wide range of arterial flow outputs. The device was comprised of mechanical and electrical units. The mechanical unit contained a servo-motor (MDFKS 056-23 190, Lenze, Germany), a planetary gearbox (MPRN 01, VOGEL, Germany), a ball screw (SFI2005, COMTOP, Taiwan) and a cylinder tank. The electronic unit contained a microcontroller (ATMega128, Atmel AVR®, USA) for the control of the rotational pattern and speed of the servo-motor and consequent movement of the piston (Fig. 11). Due to the frequency response of the servo-motor (200 Hz) and the sampling rate of the microcontroller (1 m s), there were no limitations for producing flow pulses similar to those of human arteries. The inlet flow wave was produced through the computer interface based on previously published data of the brachial artery [24]. According to the considered flow wave, the maximum and minimum flow rates occurred at $\frac{t}{T} = 0.08$ and $\frac{t}{T} = 0.28$, respectively. Also, the mean flow rate was 4.92 (ml s^{-1}) [24].

To compare the flow wave produced by the pump to the flow wave at the inlet of the elastic tube, a rotameter with the range of 0–15 (ml s^{-1}) and a digital camera with accuracy of 80 (fps) were utilized. Results indicated negligible differences between the produced and measured flow, as demonstrated in Fig. 11b.

To study effects of arterial wall elasticity on blood flow parameters, an elastic tube with a defined stiffness modulus
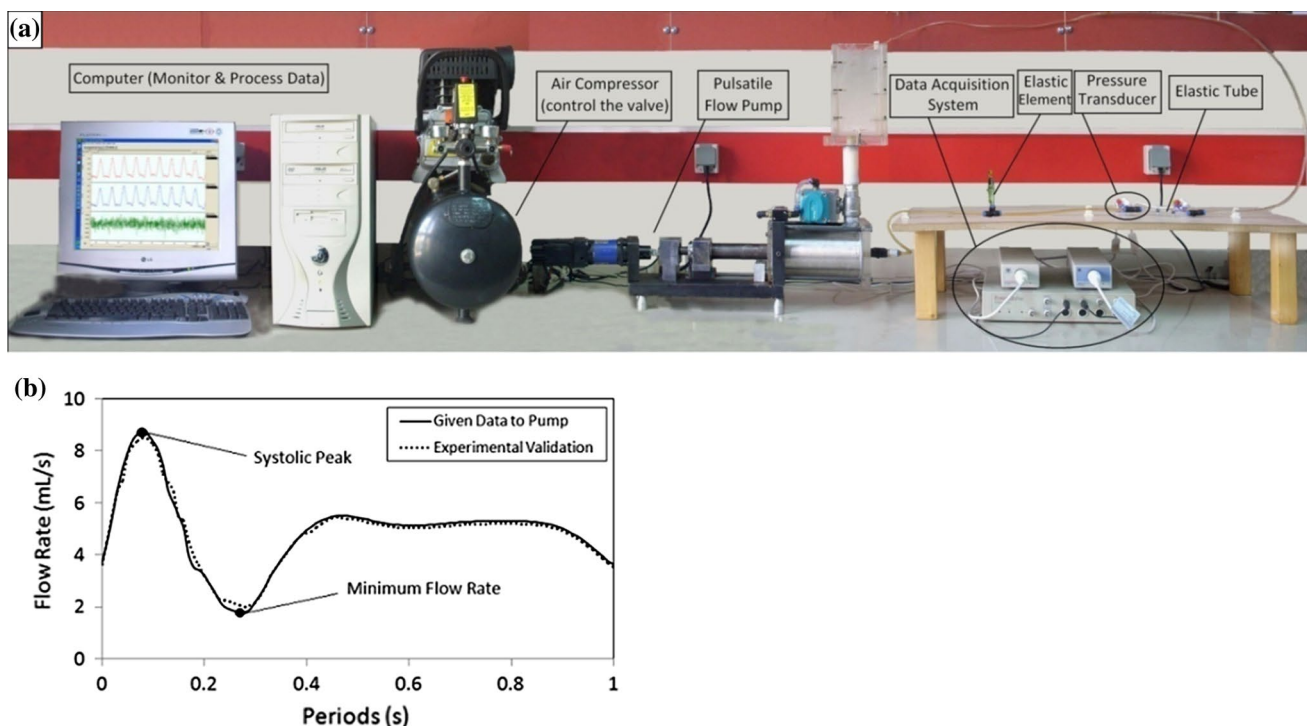

Fig. 11 **a** Overall view of experimental setup, **b** comparison of flow waves as the output of the pump to the inlet of the test specimen

was used. For biological applications, medical grade silicon tubes have been used with differing dimensions and mechanical properties. In this study, an elastic tube (D-34209, B.Braun®, Switzerland) with an inside diameter of 4.7 (mm) and wall thickness of 0.9 (mm) was used. This tube is comparable to an average human brachial artery with internal diameter and thickness of 4.5 (mm) and 0.83 (mm), respectively [40].

Mechanical properties of the tube were measured by a Universal Testing Machine (HCR 400-25, Zwick/Roell, Germany). The stress–strain relationship of the tube was similar to that of an arterial wall tissue with a hardening behavior, which is caused by elevation of pressure. Arterial walls within the human body experience pressure induced by circumferential strain pulse (diastole–systole) up to 10 % throughout the arterial tree [44]. For biological strain range, the elastic tube behaved with a linear stress–strain relationship. Hence, the stiffness modulus of the tube was considered as the slope of the curve within the aforementioned strain range. Results indicated elastic modulus of 463 (kPa) and Poisson's ratio of 0.42 for the tube, which is similar to those of an average human brachial artery: 460 (kPa) and 0.42, respectively [40].

To produce stenosis, an external square metal housing and four bolts were used to adjust various area reductions (Fig. 2c). Due to the wall elasticity, significant thickness of the tube, and luminal pressure, it is assumed that the inner profile of the tube remains almost circular.

The data acquisition and processing system contained two pressure transducers (MLT0670, ADInstruments, Australia) that were used with the operational pressure range of $50-300$ (mm Hg) (resolution of ± 0.1 (mm Hg)) and a processing unit connected to a computer. Each of the transducers was connected to a separate amplifier (ML117 BP Amp, ADInstruments™, Australia) in order to amplify the output signals before being processed. The amplifiers were connected to the main data processing unit (Powerlab/4SP, ADInstruments, Australia) by MLAC05 cables. The output pressure pulses were visualized using *Chart for Windows™ v5.0.1* software in real time. The time lag between inlet and outlet pressure pulses was considered in evaluation of the pressure difference wave and is influential in calculation of shear and circumferential stresses. Such lag is due to pulse propagation within the distensible artery and depends on elastic modulus of the tube wall.

The experimental setup included elastic and resistant elements, placed before and after the elastic tube, respectively, as presented in Fig. 11. In order to resemble physiological data for the specific flow rate, we utilized the variable valve and the elastic element to regulate the pressure pulse and mean flow. In cardiovascular system, coupling of the heart to the aorta is of great importance. The highly distensible aortic root and ascending aorta play an essential role in this coupling, leading to a continuous aortic flow and proper function of the aortic tree. Such effect is described in the Windkessel model as the elastic element [44]. In order to adjust the amplitude of pressure pulses, an elastic element was used in between the pump and the elastic tube to control the pressure to make it comparable to diastolic–systolic pulse of a typical brachial artery. The mean value of the pressure pulse was tuned by a resistant element placed after the elastic tube. Such element represented the existing hemodynamic peripheral resistance of the distal circulation.

Governing equations

Governing equations of the fluid field: Continuity and momentum equations of Newtonian fluid with negligible body forces are described as:

$$\begin{cases} \rho_f \partial_t v_f + \rho_f v_f \cdot \nabla v_f - \mathrm{div} T(v_f, P_f) = C \\ \mathrm{div} v_f = 0 \end{cases} \tag{2}$$

which v_f (x,t) is the fluid velocity vector, P_f (x,t) is the fluid pressure, and ρ_f is the fluid density. The term $\mathbf{T}(v_f, P_f) = -P_f \mathbf{I} + 2\mu_f \mathbf{D}(v_f)$ describes the Cauchy stress tensor, in which μ_f describes the fluid viscosity and $\mathbf{D}(v_f) = \frac{1}{2}\left(\nabla v_f + (\nabla v_f)^T\right)$ is the deformation rate tensor.

Governing equations of the wall Large deformation theory was used to model arterial wall deformation. The continuity and momentum equations of elastodynamics for the wall are as follows:

$$\begin{cases} \rho_s \ddot{\mathbf{u}} = \nabla.\sigma_s + \rho_s f \\ \frac{\partial \rho_s}{\partial t} + \nabla.\rho_s \mathbf{u}_s = 0 \end{cases} \tag{3}$$

where $\mathbf{u}_s$ is the wall displacement vector, σ_s is the Cauchy stress tensor, $\mathbf{f}$ is the body force vector, and ρ_s is the wall density.

The Green–Lagrange strain was used due to large deformation of the wall. To do so, corresponding stress measure that relates stresses to the reference situation was adopted. The resulting symmetric stress tensor $\mathbf{S}$, called the second Piola–Kirchhoff stress tensor, is a proper description for large deformation computations. To determine the stress, Cauchy stress has to be computed by:

$$\sigma_s = \frac{1}{J} \mathbf{F}.\mathbf{S}.\mathbf{F}^T \tag{4}$$

where $\mathbf{F} = \left(\nabla_0 \vec{x}\right)^T$ is the deformation gradient tensor with respect to a reference configuration of the solid and J is the determinant of $\mathbf{F}$. Thus, the Green–Lagrange strain tensor E could be defined as:

$$\mathbf{E} = \frac{1}{2}\left(\mathbf{F}^T \mathbf{F} - 1\right) \tag{5}$$

Governing equations of the fluid–solid coupling: In order to obtain a complete FSI coupled system, two coupling conditions on the fluid–solid interface are required. The first condition describes the fluid–solid interface as a Dirichlet boundary for the fluid, i.e., the preset velocity values of the fluid must be equal to the structural nodal velocities, as is given by:

$$\mathbf{v}_f = \dot{\mathbf{u}}_s \quad \text{on } T^c \tag{6}$$

where T^c represents the interface between fluid and solid.

The second condition indicates that the fluid–solid interface is treated as a Neumann boundary for the solid, i.e., the solid boundary traction at the reference configuration, t_{0s}, is given by acting surface loads from the fluid boundary tractions, t_f, on interface at reference time as:

$$t_{0s} = -\frac{dT_{ts}}{dT_{0s}} t_f \quad \text{on } T_{0s}^c \tag{7}$$

where dT is definition of differentiation due to load interchange on interface and subscripts 0 and t describe reference and changed configurations of fluid–solid interface, respectively. The negative sign refers to opposite directions of the normal vectors on the interface of fluid and structure with respect to a reference configuration. The formulation implies that the fluid boundary moves with the structure.

Numerical modeling

To further study effects of luminal stenosis on circumferential and wall shear stress waves together with the phase shift between them and the value of oscillation of shear stress, numerical models were analyzed, using fluid–structure interaction (FSI) method. The input data for models were based on experimental results. Models included degrees of severity of 20, 50 and 80 %. Models were developed and solved using FSI method by means of ANSYS CFX software as an axisymmetric model due to the symmetric geometry of an elastic tube and the applied stenosis within the experiment. Mechanical properties of the arterial wall (as the solid portion of model) and fluid field were allocated as described previously. The wall section was meshed with 8-node hexahedral mesh and the fluid field with 4-node tetrahedral mesh. Due to presence of stenosis, the mesh number was raised especially at stenosis site due to high stress gradient. A sensitivity analysis was performed for mesh number, and the optimized number was obtained in such a way that by elevation of mesh number, changes in resultant parameters were negligible. To verify grid independency, five grid sizes were applied for the model with 50 % stenosis. Table 1 shows the convergence of systolic average velocity at throat at systolic peak. A maximum difference of 1.6 % was observed when the density of 534 (elements mm^{-3}) was replaced by the density

Table 1 Average systolic velocity at stenosis throat for severity of 50 % for five grid sizes

Elements mm 3	152	291	347	423	534
Velocity (m s^{-1})	0.989	0.995	1.007	1.010	1.011

of 291 (elements mm^{-3}), and was assumed to be acceptable using the latter. For the solid domain due to the thin wall the density of 150 elements/mm^3 was implemented.

Figure 2 shows part of a typical model of the stenotic artery with pre-stenotic and stenotic lengths of $Z_1 = 30$ (mm), $Z_2 = 40$ (mm) and total length of L = 110 (mm) for development of flow before and after luminal obstruction.

The applied flow wave [24] and the outlet pressure wave (P_2) measured and recorded in each set of experiments were used as two boundary conditions to the each respective model. The axial displacement of the arterial wall was restricted at inlet and outlet boundaries, as designed for the experiment. To reach a proper convergence, the model was pressurized to 80 (mm Hg) for 1 s and then the model was solved for five cardiac cycles with the defined period a cardiac cycle. To ensure convergence of results for all models, results of numerical models were calculated for the fifth cycle. This was achieved by sensitivity analysis of number of cycles based on minimal cycle to cycle change of results. Since resultant stresses (i.e., WSS and CS) for the fifth cycle were almost the same as the fourth cycle, we consider the fifth cycle for all reported stress results. The boundary conditions were applied far from the stenosis (5D from each end of the tube) to avoid the circumferential effects. Since for this region, the cross-sectional area is the same as the exit region, the additional pressure drops both in experiments and in numerical analysis were assumed to be negligible compared to that of the stenosis. The results were recorded from the fifth cycle at the mid-cross section of the arterial model to determine spatially averaged situation. Resultant parameters included inlet and outlet pressure pulses and pressure difference wave, wall shear and circumferential stress waves, oscillatory shear index and angular phase difference between WSS and CS in different scales of stenosis. The parameter OSI is defined as follows [5]:

$$\text{OSI} = \frac{1}{2}\left(1 - \frac{|\tau|}{|\overline{\tau}|}\right) \tag{8}$$

where $|\tau|$ is the magnitude of WSS and $\overline{\tau}$ is the mean value of WSS.

The computational inlet pressure wave (P_1), compared to the P_1 wave measured and recorded in each set of experiment, was chosen as the criteria of validation of the model, as we chose appropriate P_2 and then solved the problem numerically to obtain P_1. Results showed a good agreement with both experimental and published data [24].

To analyze the phase difference between wall shear stress and circumferential stress waves a mathematical algorithm based on the discrete Fourier transform was carried. First we need to determine the waveforms of the diameter variation, D(t), and the wall shear stress, WSS(t), at a particular site of interest in the model. We decompose each waveform into a Fourier series with an amplitude and phase angle for each harmonic. The phase angle difference between the first harmonic of D(t) and WSS(t) is defined as the SPA. We can also define the SPA for the higher harmonics as we calculated in this study. Since a temporal variation of circumferential stretch is nearly in phase with that of pressure, we can approximate circumferential stretch by pressure variation [40]. The parameter SPA can be defined as follows:

$$\text{SPA} = \varphi(D - \tau) = \varphi(D - Q) - \varphi(\tau - Q) \simeq \varphi(P - Q) - \varphi(\tau - Q) \tag{9}$$

References

1. Aristokleous N, Kontopodis NG, Tzirakis K, Ioannou CV, Papaharilaou Y (2015) Hemodynamic impact of abdominal aortic aneurysm stent-graft implantation-induced stenosis. Med Biol Eng Comput 54:1–10
2. Bassiouny HS, White S, Glagov S, Choi E, Giddens DP, Zarins CK (1992) Anastomotic intimal hyperplasia: mechanical injury or flow induced. J Vasc Surg 15:708–717
3. Berger S, Jou L (2000) Flows in stenotic vessels. Annu Rev Fluid Mech 32:347–382
4. Caro C, Fitz-Gerald J, Schroter R (1971) Atheroma and arterial wall shear observation, correlation and proposal of a shear dependent mass transfer mechanism for atherogenesis. Proc R Soc Lond B: Biol Sci 177:109–133
5. Cebral JR, Yim PJ, Löhner R, Soto O, Choyke PL (2002) Blood flow modeling in carotid arteries with computational fluid dynamics and MR imaging. Acad Radiol 9:1286–1299
6. Chen J, Lu X-Y (2006) Numerical investigation of the non-Newtonian pulsatile blood flow in a bifurcation model with a nonplanar branch. J Biomech 39:818–832
7. Dammers R, Stifft F, Tordoir JH, Hameleers JM, Hoeks AP, Kitslaar PJ (2003) Shear stress depends on vascular territory: comparison between common carotid and brachial artery. J Appl Physiol 94:485–489
8. Dancu MB, Tarbell JM (2006) Large negative stress phase angle (SPA) attenuates nitric oxide production in bovine aortic endothelial cells. J Biomech Eng 128:329–334
9. de Carvalho ACC, Lopes RD, de Paola AA (2015) Atrial fibrillation and stroke prevention. In: Andrade JP, Pinto FJ, Arnett DK (eds) Prevention of cardiovascular diseases. Springer, pp 261–276
10. Gertz SD, Uretsky G, Wajnberg RS, Navot N, Gotsman MS (1981) Endothelial cell damage and thrombus formation after partial arterial constriction: relevance to the role of coronary artery spasm in the pathogenesis of myocardial infarction. Circulation 63:476–486
11. Ghalichi F, Deng X, De Champlain A, Douville Y, King M, Guidoin R (1998) Low Reynolds number turbulence modeling of blood flow in arterial stenoses. Biorheology 35:281–294
12. Gingrich WK, Cho YI, Shyy W (1992) Effect of aspect ratio on laminar heat transfer behavior of a non-Newtonian fluid in an electronics coldplate. Int Commun Heat Mass Transf 19:311–325
13. Hayashi K, Imai Y (1997) Tensile property of atheromatous plaque and an analysis of stress in atherosclerotic wall. J Biomech 30:573–579
14. Holzapfel GA, Sommer G, Regitnig P (2004) Anisotropic mechanical properties of tissue components in human atherosclerotic plaques. J Biomech Eng 126:657–665
15. Hughes P, How T (1995) Flow structures at the proximal side-to-end anastomosis. Influence of geometry and flow division. J Biomech Eng 117:224–236
16. Kaazempur-Mofrad M, Wada S, Myers J, Ethier C (2005) Mass transport and fluid flow in stenotic arteries: axisymmetric and asymmetric models. Int J Heat Mass Transf 48:4510–4517
17. Kabinejadian F, Cui F, Su B, Danpinid A, Ho P, Leo HL (2015) Effects of a carotid covered stent with a novel membrane design on the blood flow regime and hemodynamic parameters distribution at the carotid artery bifurcation. Med Biol Eng Comput 53:165–177
18. Kleinstreuer C, Lei M, Archie J (1996) Flow input waveform effects on the temporal and spatial wall shear stress gradients in a femoral graft-artery connector. J Biomech Eng 118:506–510
19. Lee K, Xu X (2002) Modelling of flow and wall behaviour in a mildly stenosed tube. Med Eng Phys 24:575–586
20. Liepsch D (2002) An introduction to biofluid mechanics—basic models and applications. J Biomech 35:415–435
21. Liu B (2007) The influences of stenosis on the downstream flow pattern in curved arteries. Med Eng Phys 29:868–876
22. Loree HM, Kamm R, Stringfellow R, Lee R (1992) Effects of fibrous cap thickness on peak circumferential stress in model atherosclerotic vessels. Circ Res 71:850–858
23. Matsuzaki Y, Ikeda T, Matsumoto T, Kitagawa T (1998) Experiments on steady and oscillatory flows at moderate Reynolds numbers in a quasi-two-dimensional channel with a throat. J Biomech Eng 120:594–601
24. Nichols W, O'Rourke M (2005) McDonald's blood flow in arteries, 5th edn. Arnold, London
25. Niroomand H, Tafazzoli M, Ghalichi F (2007) Flow characteristics in elastic arteries using a fluid-structure interaction model. Am J Appl Sci 4:516–524
26. Ojha M (1994) Wall shear stress temporal gradient and anastomotic intimal hyperplasia. Circ Res 74:1227–1231
27. Pontrelli G, Rossoni E (2003) Numerical modelling of the pressure wave propagation in the arterial flow. Int J Numer Method Fluids 43:651–671
28. Qiu Y, Tarbell JM (2000) Numerical simulation of pulsatile flow in a compliant curved tube model of a coronary artery. J Biomech 122:77–85
29. Sadeghi M, Shirani E, Tafazzoli-Shadpour M, Samaee M (2011) The effects of stenosis severity on the hemodynamic parameters—assessment of the correlation between stress phase angle and wall shear stress. J Biomech 44:2614–2626
30. Sarmast M, Niroomand-Oscuii H, Ghalichi F, Samiei E (2014) Evaluation of the hemodynamics in straight 6-mm and tapered 6-to 8-mm grafts as upper arm hemodialysis vascular access. Med Biol Eng Comput 52:797–811
31. Slager C, Wentzel J, Gijsen F, Schuurbiers J, Van der Wal A, Van der Steen A, Serruys P (2005) The role of shear stress in the generation of rupture-prone vulnerable plaques. Nat Clin Pract Cardiovas Med 2:401–407
32. Smedby Ö (1997) Do plaques grow upstream or downstream? An angiographic study in the femoral artery. Arterioscler Thromb Vasc Biol 17:912–918
33. Sousa LC, Castro CF, António CC, Santos AMF, dos Santos RM, Castro PMA, Azevedo E, Tavares JMR (2014) Toward hemodynamic diagnosis of carotid artery stenosis based on ultrasound image data and computational modeling. Med Biol Eng Comput 52:971–983

34. Tada S (2010) Numerical study of oxygen transport in a carotid bifurcation. Phys Med Biol 55:3993

35. Tada S, Tarbell J (2005) A computational study of flow in a compliant carotid bifurcation–stress phase angle correlation with shear stress. Ann Biomed Eng 33:1202–1212

36. Tang D, Yang C, Walker H, Kobayashi S, Ku DN (2002) Simulating cyclic artery compression using a 3D unsteady model with fluid–structure interactions. Comput Struct 80:1651–1665

37. Taylor CA, Hughes TJ, Zarins CK (1999) Effect of exercise on hemodynamic conditions in the abdominal aorta. J Vasc Surg 29:1077–1089

38. Tu C, Deville M (1996) Pulsatile flow of non-Newtonian fluids through arterial stenoses. J Biomech 29:899–908

39. Valencia A, Baeza F (2009) Numerical simulation of fluid–structure interaction in stenotic arteries considering two layer nonlinear anisotropic structural model. Int Commun Heat Mass Transf 36:137–142

40. van der Heijden-Spek JJ, Staessen JA, Fagard RH, Hoeks AP, Boudier HAS, Van Bortel LM (2000) Effect of age on brachial artery wall properties differs from the aorta and is gender dependent a population study. Hypertension 35:637–642

41. Vukicevic AM, Stepanovic NM, Jovicic GR, Apostolovic SR, Filipovic ND (2014) Computer methods for follow-up study of hemodynamic and disease progression in the stented coronary artery by fusing IVUS and X-ray angiography. Med Biol Eng Comput 52:539–556

42. Wada S, Koujiya M, Karino T (2002) Theoretical study of the effect of local flow disturbances on the concentration of low-density lipoproteins at the luminal surface of end-to-end anastomosed vessels. Med Biol Eng Comput 40:576–587

43. Yakhshi-Tafti E, Tafazzoli-Shadpour M, Alavi SH, Mojra A (2009) Coupled fluid-wall modelling of steady flow in stenotic carotid arteries. J Med Eng Technol 33:544–550

44. Y-c Fung (2013) Biomechanics: circulation. Springer, New York

Mohammad Tafazzoli-Shadpour is Associate Professor of Department of Biomedical Engineering at Amirkabir University of Technology.

Hamed Alavi is postdoctoral scholar at University of California, Irvine. His responsibilities are included: animal study of the world's first hybrid self-regenerative heart valve, in collaboration with UC Irvine School of Medicine, leading a team of scientists at UC Irvine and durability testing a novel nitinol mesh-made heart valve using an accelerated wear testing system, along with computational simulation of the nitinol valves for enhancement of stress distribution over the leaflets and to increase their fatigue life, managing a team of scientists at UC Irvine.

Milad Samaee is a second year Ph.D. student in mechanical engineering at Oklahoma State University. Milad's research interests are in biomechanics and biomedical devices. He is currently working on cardiac fluid dynamics and metachronal paddling projects.